Master's Thesis

A new two-dimensional spin-configuration-dependent rate-controlled Monte Carlo simulation model: microstructural evolution and application to coarsening of bicontinuous porous metal

Gaeun Son

Department of Materials Science and Engineering

Graduate School of UNIST

2019

A new two-dimensional spin-configuration-dependent rate-controlled Monte Carlo simulation model: microstructural evolution and application to coarsening of bicontinuous porous metal

Gaeun Son

Department of Materials Science and Engineering

Graduate School of UNIST

A new two-dimensional spin-configuration-dependent rate-controlled Monte Carlo simulation model: microstructural evolution and application to coarsening of bicontinuous porous metal

A thesis/dissertation
submitted to the Graduate School of UNIST
in partial fulfillment of the
requirements for the degree of
Master of Science

Gaeun Son

7/12/ 2019
Month/Day/Year of submission

Approved by

Advisor
Sukbin Lee

A new two-dimensional spin-configuration-dependent rate-controlled Monte Carlo simulation model: microstructural evolution and application to coarsening of bicontinuous porous metal

Gaeun Son

This certifies that the thesis/dissertation of Gaeun Son is approved.

7/12/2019
Month/Day/Year of submission

signature

Advisor: Sukbin Lee

signature

Thesis Committee Member #1: Kisuk Lee

signature

Thesis Committee Member #2: Ju-young Kim

Abstract

The coarsening of the two-phase, bicontinuous microstructure via surface diffusion is simulated using a two-dimensional and a three-dimensional Monte Carlo (MC) model. We investigate the morphological evolution and coarsening kinetics of microstructures during phase separation. A conventional spin-exchange Kawasaki dynamic has been used to predict the evolution of the microstructures via the diffusion-controlled mechanism. Here, we suggest a new Monte Carlo model where the control of the diffusion rate is achieved considering the configurational changes as a consequence of the spin-exchange. To verify the proposed model, the microstructural characterization using simulation snapshot patterns, the intercept method, the structure factor and the pair correlation function, is performed to measure the characteristic length and its temporal evolution. From the resultant temporal evolution of the characteristic length, it is found that the dynamics of the system with zero bulk diffusivity achieves a higher value of kinetic exponent of ~ 4 than the conventional Kawasaki dynamics model over the intermediate temperature range. Also, we found that the area fraction of the system strongly affects the evolution of microstructure. Lastly, we compare the results from the proposed model to the coarsening of a porous metal system. Kinetic analysis on nanoporous gold (np-Au) samples, annealed at 450 and 600 °C, confirms the prediction of the model. The coarsening probability ratio of np-Au between two annealing temperatures, calculated from the reported activation energy for coarsening of np-Au, is comparable to that of the model, signifying that the simulation successfully mimics the kinetic evolution of the thermally coarsened np-Au via surface diffusion.

Keywords: Monte Carlo simulation; Two-phase system; Coarsening kinetics; Bicontinuous microstructure; Surface diffusion;

Contents

Table of figures

I. Introduction

An understanding of microstructural evolution, which contains morphological changes and kinetics of coarsening is critical to all materials. The shape, size and spatial arrangement of precipitates in microstructure play an important role in determining the physical properties of materials. Especially in metallic materials, the introduction of defect such as precipitates harden the metal alloys. It is of great importance to know the nucleation, growth, and phase separation under various conditions of temperature and volume fraction.

In the early 1960s, Lifshitz and Slyozov [1] and Wagner [2] developed a first formal theory of coarsening (i.e. LSW theory), assumed that coarsening occurred through the movement of a single sedimentary atom, and that the atom diffused from a small precipitate was finally condensed into a larger precipitate.

$$\overline{R}^3 - \overline{R_0}^3 = kt \tag{1}$$

where $\overline{R}$ is the average particle size, $\overline{R_0}$ is the average size at t = 0, and k is the rate constant. LSW theory predicts linear relationship between the cube of average particle size and time t because of predominant evaporation – condensation mechanism.

The Monte Carlo Ising model representing two-phase systems has been used since the early 1970s to represent phase separation in alloys [3-7]. These models are composed of two types of atom, A-atom and B-atom, and the dynamics was described by the Kawasaki dynamics [8], the stochastic exchange between A and B atoms. With the extension, each lattice site can be taken by an A-atom, a B-atom and a vacant, yielding a ternary ABV model [9-12], which the dynamics of phase separation is represented more realistically by atoms jumping into neighboring empty vacancy spaces. In contrast to the classical LSW law $\overline{R}^3 \sim kt$, they [12] expect as $\overline{R}^5 \sim kt$ because of coagulation mechanism, which is to move particles as a whole and to coalesce.

In addition, Cahn-Hilliard equation and phase-field model have been used to determine the degree of microstructure coarsening. The LSW cubic law for evaporation – condensation mechanism was confirmed by numerical simulations [13-16] using a constant-mobility Cahn-Hilliard equation. There have also been a number of studies using Cahn-Hilliard equation with scaled mobility for expressing in the case of the predominant diffusion mechanism. The two-phase microstructure with interfacial diffusion has $\overline{R}^4 \sim kt$ [17], and in the case of large diffusional mobility disparity kinetic of phase separation leads to $\overline{R}^{3.3} \sim kt$ [18].

There have been many attempts to improve the LSW theory, as well as the development of simulation models to more accurately predict the kinetics under various conditions. Here we propose the modified Monte Carlo Ising model with Kawasaki dynamics by controlling the various type of diffusion with spin swap configurations under various system temperatures and area fractions. In chapter II, we explain the backgrounds for understanding Monte Carlo simulation, and three numerical methods for calculating the characteristic lengths of microstructure. Chapter III describes the newly proposed Monte Carlo model, and the results of microstructure evolution simulation are described with comparison of Kawasaki dynamics model and the proposed model. We observe the effects of various simulation temperature and area fraction through images and kinetic analysis and verify the feasibility of the proposed research model. In chapter IV, we extend the 2D simulation model to 3D model and compare its kinetics with the results of real materials.

II. Theoretical background

2.1 Monte Carlo Ising model

In the late 1940s, the Monte Carlo simulation was developed for studying nuclear reactions, which does not proceed in some strictly predefined equations like Newton's equations of motion, but in a stochastic manner which depends on random numbers which are generated during the simulation. Therefore, it allows efficient computation of high-dimensional integrals and used in several domains, including mathematics, economy, biology, and material science. In material science, it is widely used for modeling microstructural evolution studies, such as grain growth and recrystallization in polycrystalline materials [19], coarsening in liquid phase sintering [20, 21], pore-boundary interactions [22] and phase separation of a binary alloy [23].

When a microstructure describes a binary system consisting of two components, this is called an Ising model [24, 25]. It has also been used to study the microstructural evolution of grain boundaries or the behavior of bicrystals, since the two components are represented by the two types of spin, $s_i \in \{-1, 1\}$, where i labels the lattice site.

2.1.1 Hamiltonians

The Hamiltonians of the system is expressed as the sum of the interfacial energy between all possible interacting neighboring pixel pairs. There is a boundary between different type of spins, and there is no boundary between the same type of spins as in the following,

$$\begin{aligned} e(s_i, s_j) &= 0, \qquad s_i = s_j \\ e(s_i, s_j) &= \mathrm{J}, \qquad s_i \neq s_j \end{aligned} \tag{2}$$

where i is a site, j is its neighboring site, and J is an interfacial energy of the system. Therefore, we can write the total energy of the system as the following equation,

$$E = \frac{1}{2}\sum_{i}^{N}\sum_{j}^{z} e(s_i, s_j) \tag{3}$$

where N represents the total number of lattice sites in the system, and z is the number of nearest neighbors, which depends on the dimension and type of lattice. In a simple square (for two-dimensional, 2-D) and cubic (for three dimensional, 3-D) lattice, z is 8 and 26, respectively.

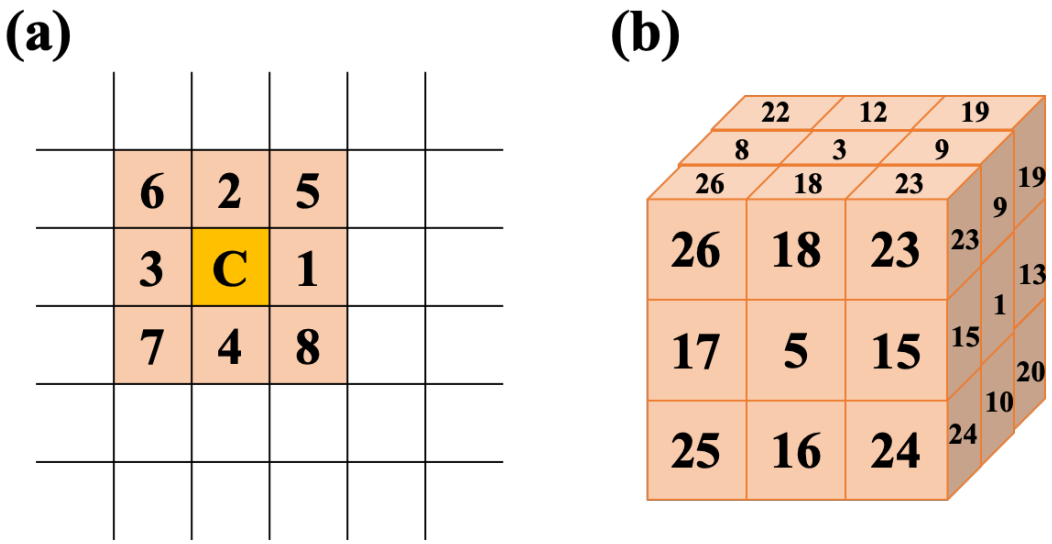

Figure 1. Coordination of neighbor sites used in the Ising model, (a) 2D square lattice, and (b) 3D cubic lattice.

2.1.2 Kawasaki dynamics

The state of the system depends on the distribution of the spins in the lattice. For the stabilization of the total energy of the system over simulation time, we can sample different states with a simple method, which is to select a site and its neighboring site as a pair randomly, to propose an exchange of spin pair, to calculate the change in energy ΔE associated with that spin swap, and to accept or reject the exchange based on ΔE. Especially Kawasaki [8] dynamics method achieves situations in which the volume fraction of each spin type is preserved by exchanging the spins with each other. Here, a lattice site and its neighboring site are chosen at random as a pair, and then the spin exchange is proposed. The ΔE before and after spin exchange is calculated, and finally the change is accepted or not using a probability function that relies on energy differences ΔE.

2.1.3 Metropolis algorithm

Metropolis algorithm [26] is one of the algorithms that have a probability function, deciding the spin-exchange whether to accept or reject. The probability is determined by the difference in energy, ΔE and follows

$$\begin{aligned} p &= \exp\left(\frac{-\Delta E}{kT}\right), && \Delta E > 0 \\ p &= 1, && \Delta E \leq 0 \end{aligned} \tag{4}$$

where k is the Boltzmann constant and T is the temperature of the system. We should compare p with random number, r chosen uniformly in the interval 0 to 1 and accept the spin-exchange if $p >$ r.

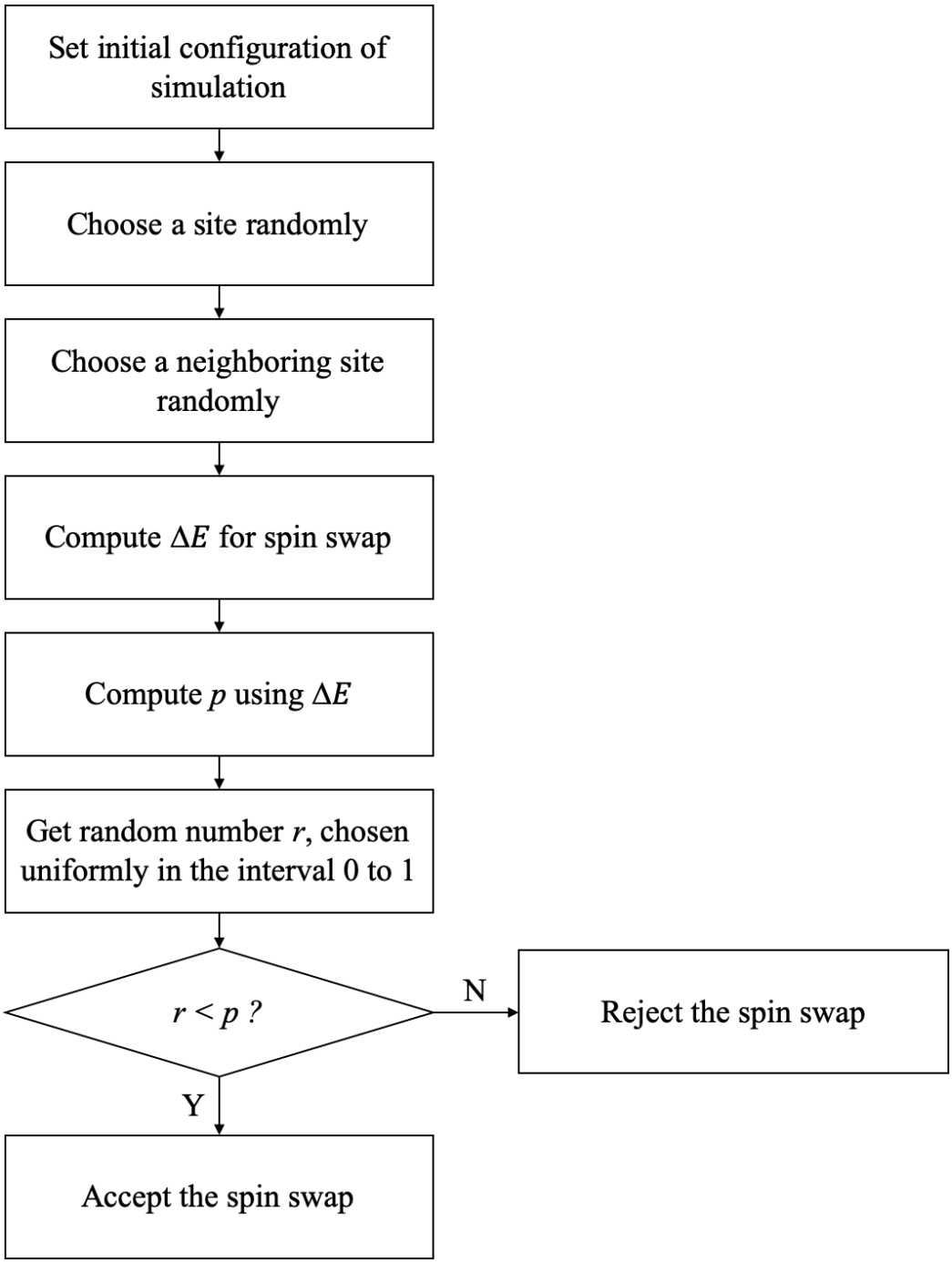

Figure 2. The algorithm for the conserved spin Ising model using Kawasaki dynamics and Metropolis algorithm.

2.1.4 Periodic boundary conditions (PBC)

Dealing with the boundary of the lattice is important because simulations always performs in finite systems. The most popular type of boundary condition is the 'Periodic Boundary Condition' (PBC), the first spin of the row sees the last spin of the row as the nearest neighbor, and vice versa. The same goes for spins at the top and bottom of the column. Figure 3 shows this procedure for a two-dimensional square lattice.

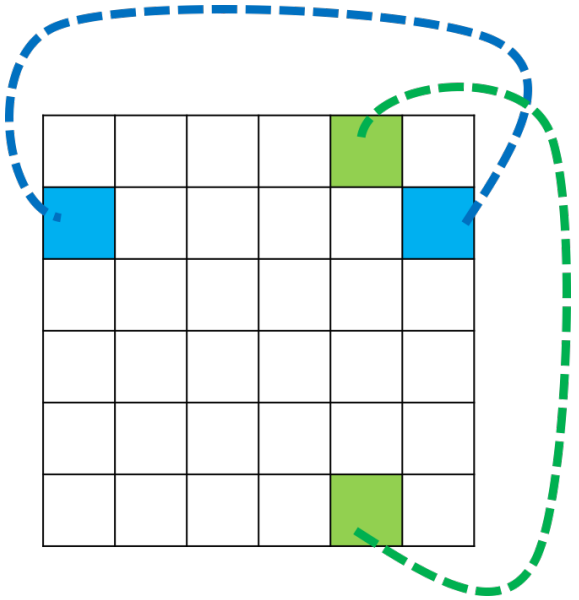

Figure 3. Periodic boundary conditions (PBC) for the 2D Ising model by assigning the nearest neighbors of each edge site to the opposite boundary edge.

2.2 Numerical methods for characteristic length of microstructure

In order to understand the kinetics of the microstructure, it is necessary to observe the changes in characteristic lengths over simulation time. Here, the characteristic length of the microstructure can be calculated in three ways: intercept method, structure factor[16, 27], and pair correlation function [13, 16].

2.2.1 Intercept method

Average Grain Intercept (AGI) method is a technique used to quantify the grain or crystal size for a given material by drawing a set of randomly positioned line segments on the micrograph. We improve this method to quantify the ligament size for a given microstructure by drawing a set of circles, measuring the size of each segment intersects a boundary, and calculating the average of all size of segments.

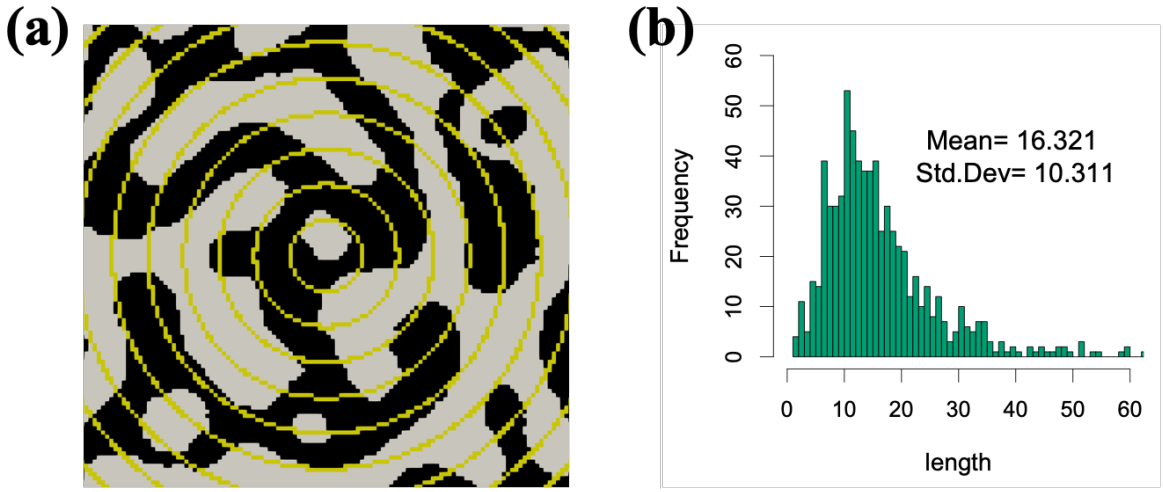

Figure 4. Intercept method for characteristic length. (a) is 2D square lattice binary microstructure, drew a set of circles (in yellow), (b) is the distribution of the size of each segment.

2.2.2 Structure factor

It has been shown [16, 27] that a two-phase morphology during coarsening can be characterized by a time-dependent structure factor $S(\boldsymbol{k}, t)$,

$$S(\boldsymbol{k}, t) = \frac{1}{N}\sum_{\boldsymbol{r}}\sum_{\boldsymbol{r}'} e^{-i\boldsymbol{k}\cdot\boldsymbol{r}}\left[C(\boldsymbol{r}+\boldsymbol{r}', t)C(\boldsymbol{r}', t) - \langle C\rangle^2\right] \quad (5)$$

with $\boldsymbol{k} = (2\pi/L)(m\boldsymbol{i} + n\boldsymbol{j})$ and $m, n = 1, 2, 3, \ldots, L$ where $N = L^2$ is the total number of pixels in the lattice. $C(\boldsymbol{r}, t)$ is a time-dependent spin value at site $\boldsymbol{r}$, and $\langle C \rangle$ denotes average of spin value over all lattice sites. Assuming the evolution to be isotropic, we compute the circularly averaged structure factor $S(k, t)$ for taking to smoothed results. The normalized structure factor $s(k, t)$ is defined as

$$s(k,t) = \frac{S(k,t)}{N[\langle C^2(\boldsymbol{r})\rangle - \langle C\rangle^2]}, \qquad k = 2\pi n/L \tag{6}$$

where $n = 0, 1, \ldots, L/2$ and for a given value of n is over a circular line defined by

$$n - \frac{1}{2} \leq \left(\frac{L}{2\pi}\right)|\boldsymbol{k}| \leq n + \frac{1}{2} \ . \tag{7}$$

There are several ways to characterize the typical length *R(t)* from structure factor. In this study we use the first moment of normalized circularly averaged structure factor $s(k, t)$, defined by

$$R_1(t) = 2\pi/k_1(t) \tag{8}$$

with

$$k_1(t) = \frac{\sum ks(k,t)}{\sum s(k,t)} \ . \tag{9}$$

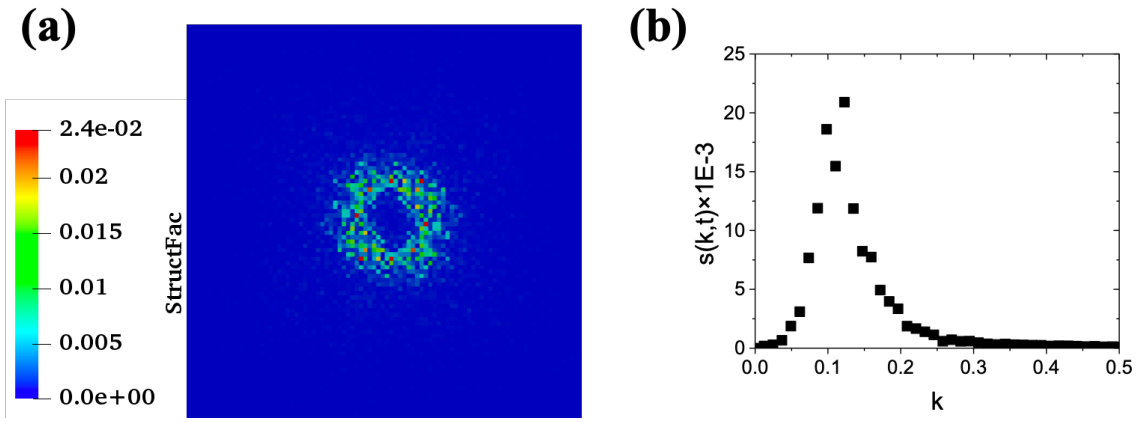

Figure 5. Structure factor for characteristic length. (a) is $S(\boldsymbol{k}, t)$ and (b) is normalized and circularly averaged structure factor $s(k, t)$.

2.2.3 Pair correlation function

Correlation of fluctuations were examined through the radial pair correlation function. The pair correlation function was defined by [16]

$$G(\boldsymbol{r},t) = \sum_{\boldsymbol{k}} e^{i\boldsymbol{k}\cdot\boldsymbol{r}}\, S(\boldsymbol{k},t) \tag{10}$$

We also consider a circularly averaged pair correlation function $G(r,t)$ and normalized pair correlation function $g(r,t)$. The normalization procedure allows us to make a more reasonable comparison for different area fractions. The location of the first zero of the real-space correlation function, $R_g(t)$, is also a good measure of the average domain size.

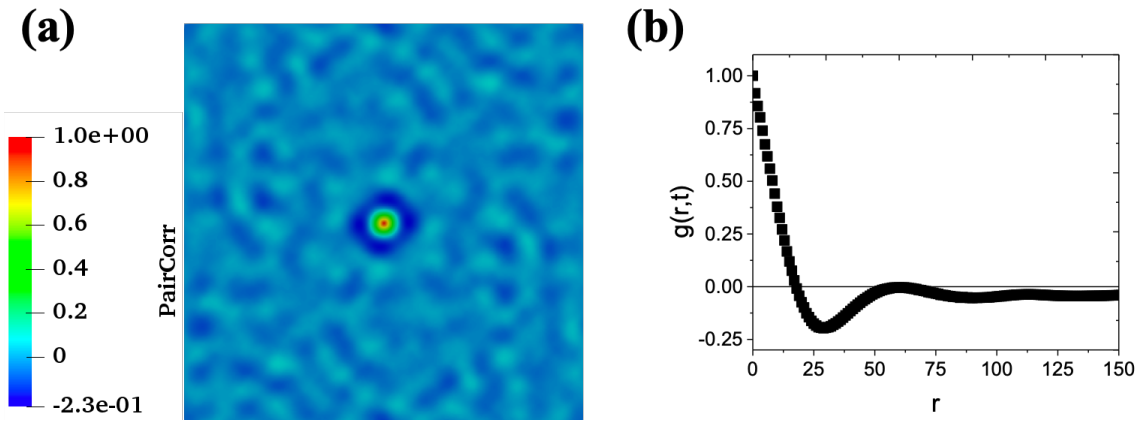

Figure 6. Pair correlation function for characteristic length. (a) is $G(\boldsymbol{r},t)$ and (b) is normalized and circularly averaged pair correlation function $g(r,t)$.

III. A new spin-configuration-dependent rate-controlled Monte Carlo

3.1 A spin-configuration-dependent rate-controlled 2D MC model

The binary systems are usually described in terms of Ising model [24, 25] with nearest neighbor interactions on a simple square lattice the sites of which are occupied by two types of spin (i.e. solid is 1 or medium is -1). The microscopic dynamics of this system are commonly described by spin-exchange method, also known as Kawasaki [8] dynamics, which the total number of solid and medium pixels remains constant. A pixel and one of its 8 interacting nearest neighbors are randomly chosen as pair, then the pixels on those sites may be interchanged with a probability which depends on the energies of the configuration before and after the exchange. A unit of simulation time represented by Monte Carlo step (MCS) is considered to have elapsed each time the total number of attempts to select a pair of pixels and the number of attempts to select a pair, regardless of the success of the spin swap.

Here, if each type of the selected pair is the same, another pair is selected since medium-medium diffusion and solid-solid diffusion are meaningless in this context. In Figure 7, solid pixel in gray and medium pixel in white, there are four possible swap processes of solid-medium pair are illustrated in example. It represents basic mechanisms that enable coarsening during simulation, are composed of surface diffusion, dissolution, bulk diffusion, and precipitation. Each pixel of a solid phase can move along the surface of a particle or be separated from it. The separated pixels can be attached to one of the particles by the random walk through a medium phase. The movement along the surface of a solid phase pixel cause the surface diffusion and the detachment of it results in the dissolution of solute. The random walk through the medium region indicates the bulk diffusion of the separated solutes, and the re-attachment of solid phase pixels onto the surface of another solid particles shows precipitation mechanism.

Whether the selected solid-medium pair performs the above swap mechanism depends on the total energy of the system, *E*. The total energy of the system equals the sum of the interfacial energy between all adjacent pixel pairs that are interactive, $e(s_i, s_j)$, where s_i and s_j are the spin numbers of the pixel pair. If $s_i = s_j$ (solid-solid or medium-medium pair), the interfacial energy between two neighboring pixels, $e(s_i, s_j)$, is defined to be zero (with an arbitrary energy unit) and if $s_i s_j < 0$ (solid-medium interfacial energy), it is 1.0. The total energy of the system, *E*, is then

$$E = \frac{1}{2}\sum_{i}^{N}\sum_{j}^{8} e(s_i, s_j) \qquad (11)$$

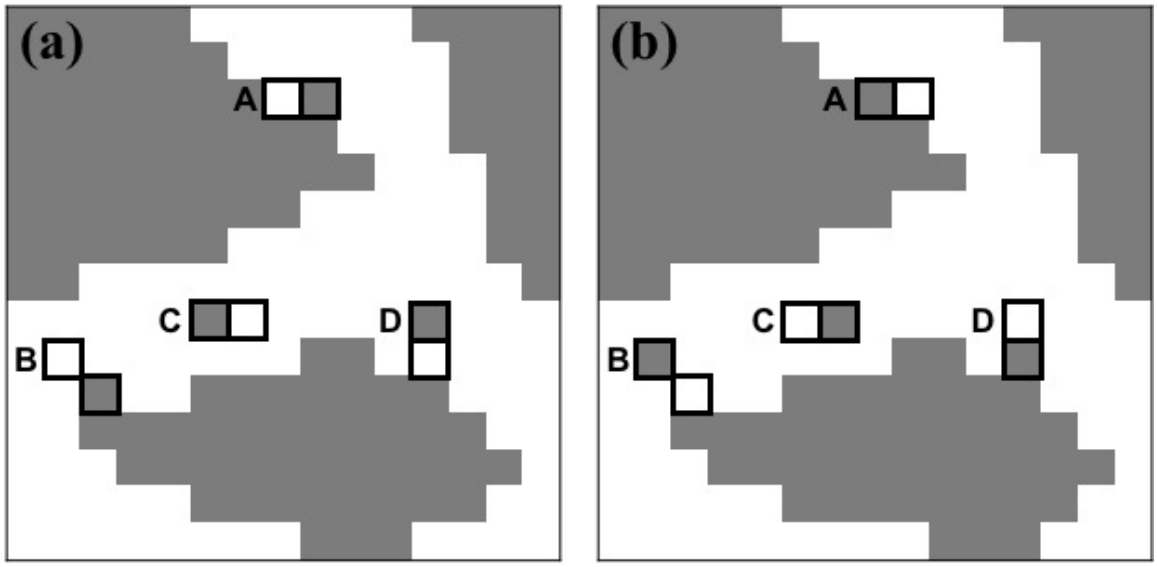

Figure 7. A schematic illustrating four possible swap mechanisms occurring during the simulations. Here, four individuals solid (in gray) — medium (in white) pixel pairs are marked with bold squares. The microstructures correspond to (a) the "old" and (b) the "new" configurations after the swap process. Note that the microstructure has evolved through (A) surface diffusion, (B) dissolution, (C) bulk diffusion, and (D) precipitation.

The difference in energy, ΔE, between a selected configuration and a new configuration should be calculated to implement the Monte Carlo simulation. A solid-medium pixel interchange generates the new configuration. This swap is accepted or not using the classical Metropolis algorithm [26] with a probability.

$$\begin{aligned} p &= \exp\left(\frac{-\Delta E}{kT}\right), \qquad \Delta E > 0 \\ p &= 1, \qquad\qquad\quad \Delta E \leq 0 \end{aligned} \tag{12}$$

where k is the Boltzmann constant and T is the temperature of the system. The energy corresponding to the system temperature is expressed in the same arbitrary energy units as those used above.

Here we improve the conventional Kawasaki dynamics to implement the various evolution of the microstructures by providing the rate barrier to four different kinds of swap mechanisms. Using the old and new configurations, we classify the type of the spin swap in one of four mechanisms and give each configuration type a rate barrier, D_{type} (i.e. D_{surf}, D_{bulk}, D_{prec}, and D_{diss}). Therefore, the spin swap is accepted or rejected using the following probability,

$$p = D_{type} \cdot \exp\left(\frac{-\Delta E}{kT}\right), \qquad \Delta E > 0$$
$$p = D_{type}, \qquad \Delta E \leq 0 \tag{13}$$

where D_{type} is a value from 0 to 1, and if all types of D_{type} are 1.0, it behaves the conventional Kawasaki dynamics.

3.2 simulation details

In this work, an initial configuration is configured by randomly assigning pixel spins in each phase under various conditions, with a solid area fraction of 0.1 to 0.5 and in the range of 0.2 to 2.2 of the system temperatures. To compare the effects of the surface diffusion, we have simulated with above conditions when all types of D_{type} is 1.0 (i.e. Kawasaki dynamics) and when only the value of D_{diss} is zero. 512 × 512 square lattices are adopted, and total simulation time of each systems is 800k Monte Carlo step (MCS). For each of these systems, five repeated simulations starting from different seeds for random number generator, have been made and the averages of quantities over the five simulations are presented below.

3.3 Results and discussions

In this section, we examine the changes in morphology and kinetics of two models, all types of D_{type} is 1.0 (let us call it "Kawasaki model") and only the value of D_{diss} is zero (let us call it "proposed model"). First, through the extracted images from vtk file format, the change in time-dependence morphologies of the two models is observed by the variation of the simulation temperature and solid area fraction. Next, we calculate the characteristic lengths using the aforementioned methods, intercept method, structure factor and pair correction function, and compare the kinetic exponents for each model.

3.3.1 Morphological evolution

3.3.1.1 Effect of temperature

Figure 8 and Figure 9 show the morphological evolution of Kawasaki model and proposed model, respectively, with 0.5 solid area fraction at four different simulation temperature. In column direction of the figure we can observe how microstructure grows at each temperature, whereas how much microstructure evolves at each simulation temperature during the same simulation time in row

direction. Both models grew faster during the same MCS at high simulation temperature, because the probability of the Metropolis algorithm was affected by kT. The larger the value of kT, the higher the probability accepting the spin swap mechanism. For this reason, spin-exchange occurs frequently when the ΔE is greater than zero, and small medium pixels are present on the solid phase and vice versa. Comparing Kawasaki model with proposed model, the growth rate of microstructure is slower under the same conditions. This is because the zero value of D_{diss} in the proposed model does not necessarily result in spin swap when the spin pair corresponding to the dissolution is selected.

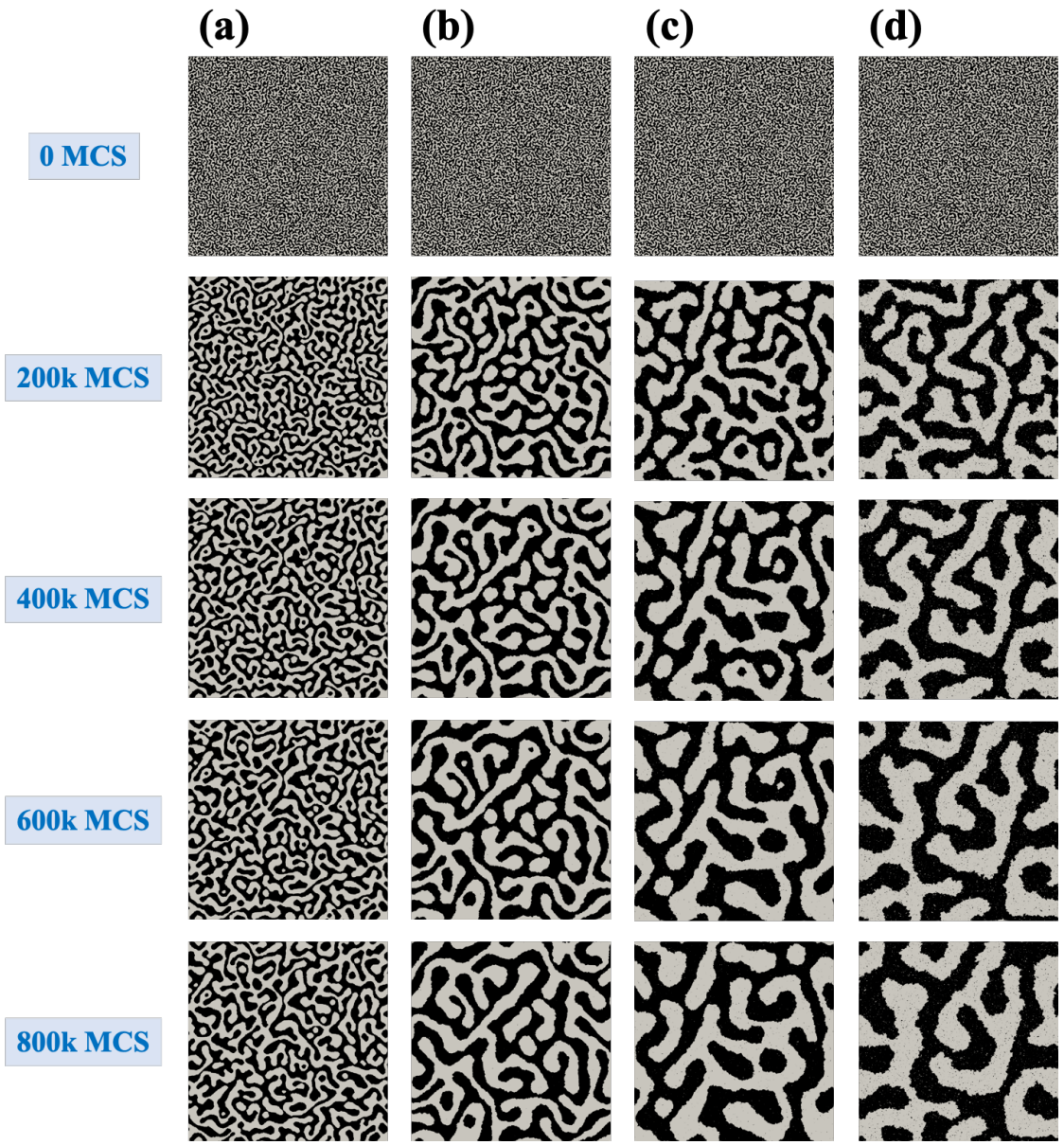

Figure 8. Snapshots of morphological changes of Kawasaki model (D_diss = 1.0) with 0.5 solid area fraction as a function of simulation time. Solid pixels and medium pixels are shown in black and gray, respectively, and simulation temperature (kT) is (a) 0.5, (b) 1.0, (c) 1.5, and (d) 2.0.

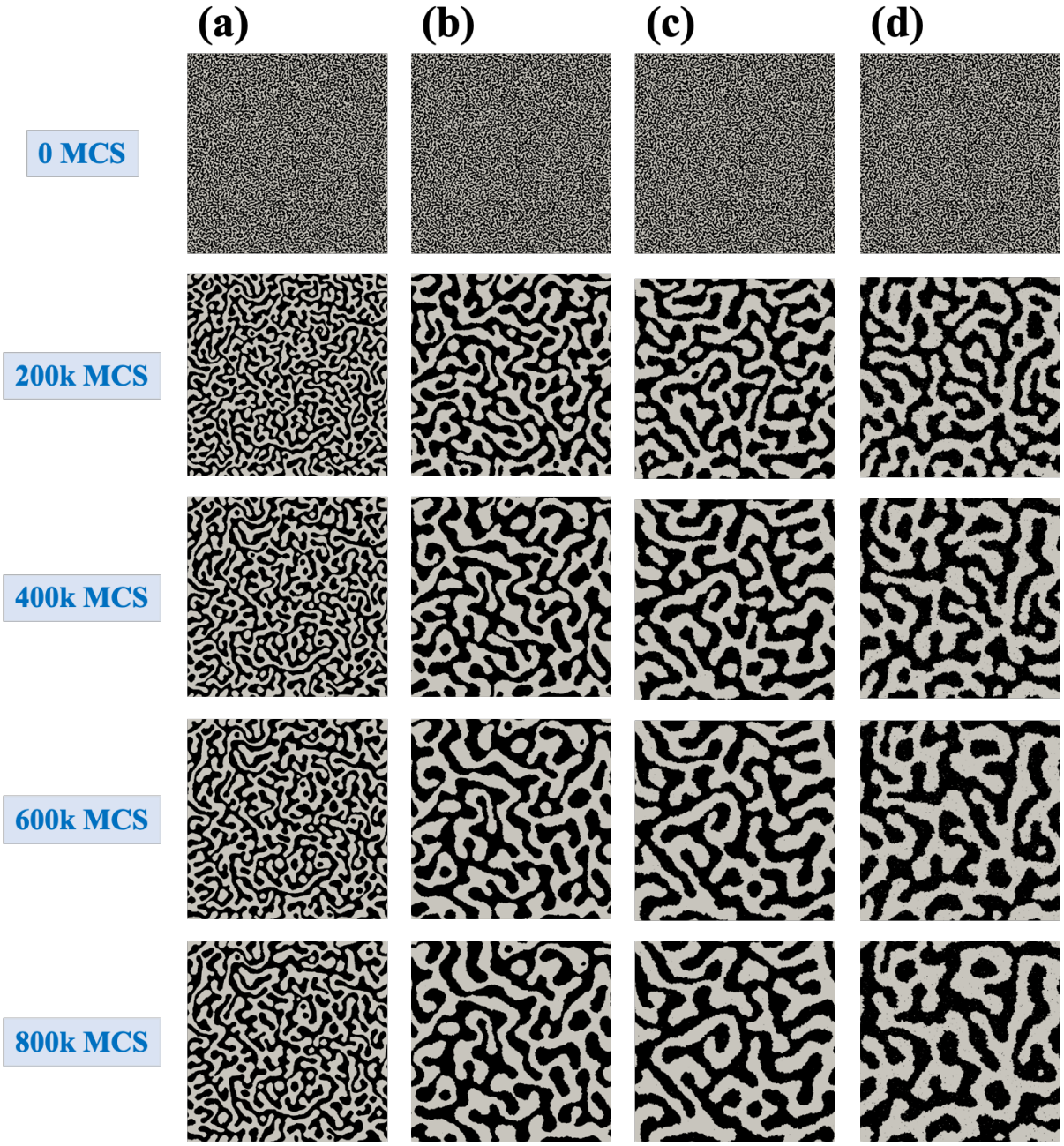

Figure 9. Snapshots of morphological changes of proposed model (D_{diss} = 0.0) with 0.5 solid area fraction as a function of simulation time. Solid pixels and medium pixels are shown in black and gray, respectively, and simulation temperature (kT) is (a) 0.5, (b) 1.0, (c) 1.5, and (d) 2.0.

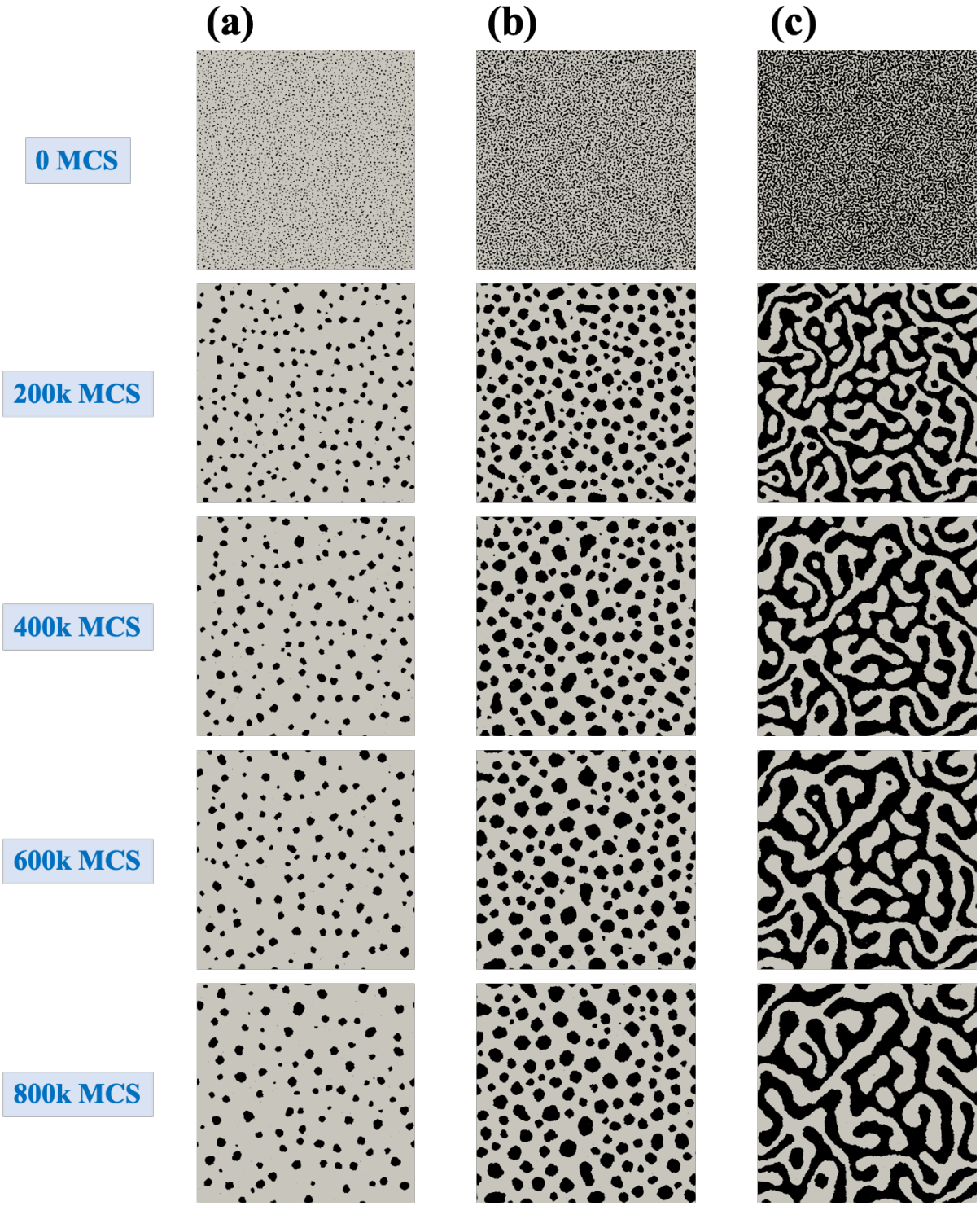

Figure 10. Snapshots of morphological changes of Kawasaki model (D_{diss} = 1.0) with kT = 1.0 as a function of simulation time. Solid pixels and medium pixels are shown in black and gray, respectively, and solid area fraction is (a) 0.1, (b) 0.3, and (c) 0.5.

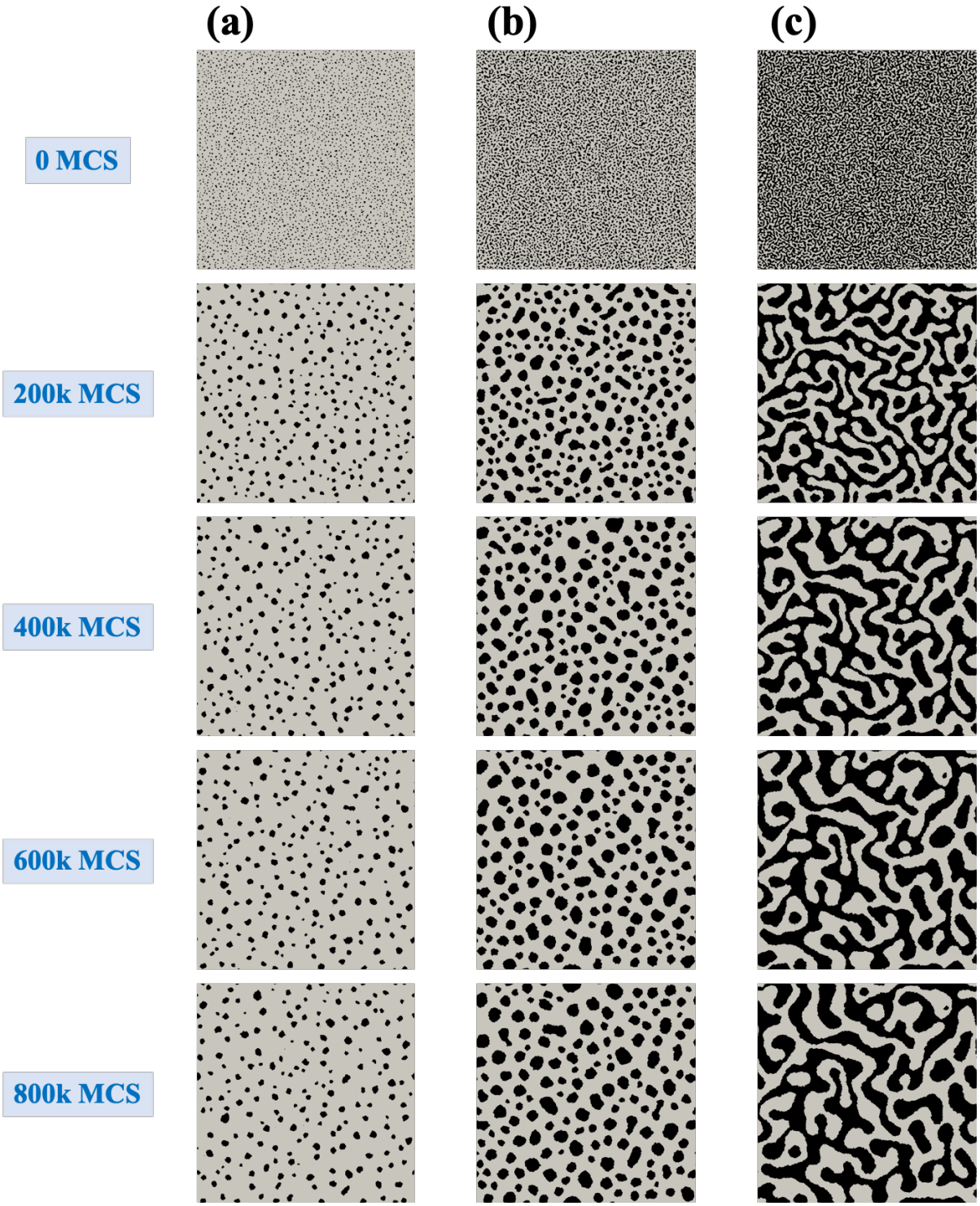

Figure 11. Snapshots of morphological changes of proposed model (D_{diss} = 0.0) with kT = 1.0 as a function of simulation time. Solid pixels and medium pixels are shown in black and gray, respectively, and solid area fraction is (a) 0.1, (b) 0.3, and (c) 0.5.

3.3.1.2 Effect of area fraction

Figure 10 and Figure 11 show the morphological evolution of Kawasaki model and proposed model, respectively, with 1.0 simulation temperature at three different solid area fractions. In column direction of the figure we can observe how microstructure grows at each solid area fraction, whereas how much microstructure evolves at each solid area fraction during the same simulation time in row direction. With fewer solid area fraction, the distance between pixel and pixel, and between particle and particle becomes distant, so it is present as a small circular shape not as a continuously connected feature.

As mentioned above, the growth of the proposed model is slower than Kawasaki model, because the effect of the value of D_{diss} of the proposed model inhibits the generation of detachment of a pixel from the particle. Without a detached pixel, the pixels move from the surface of the particles, making the accidental contact between particles to create a large one, called coalescence. The yellow circle in Figure 12 shows these phenomena. On the other hand, a detached pixel causes an Ostwald ripening, which smaller particles dissolve and deposit on larger particles in order to reach a more energetically stable state wherein the surface to area ratio is minimized. The red circle in Figure 12 – (a) is the Ostwald ripening caused by the detachment of a pixel. Thus, the Kawasaki model has another fashion for microstructural evolution than the proposed model.

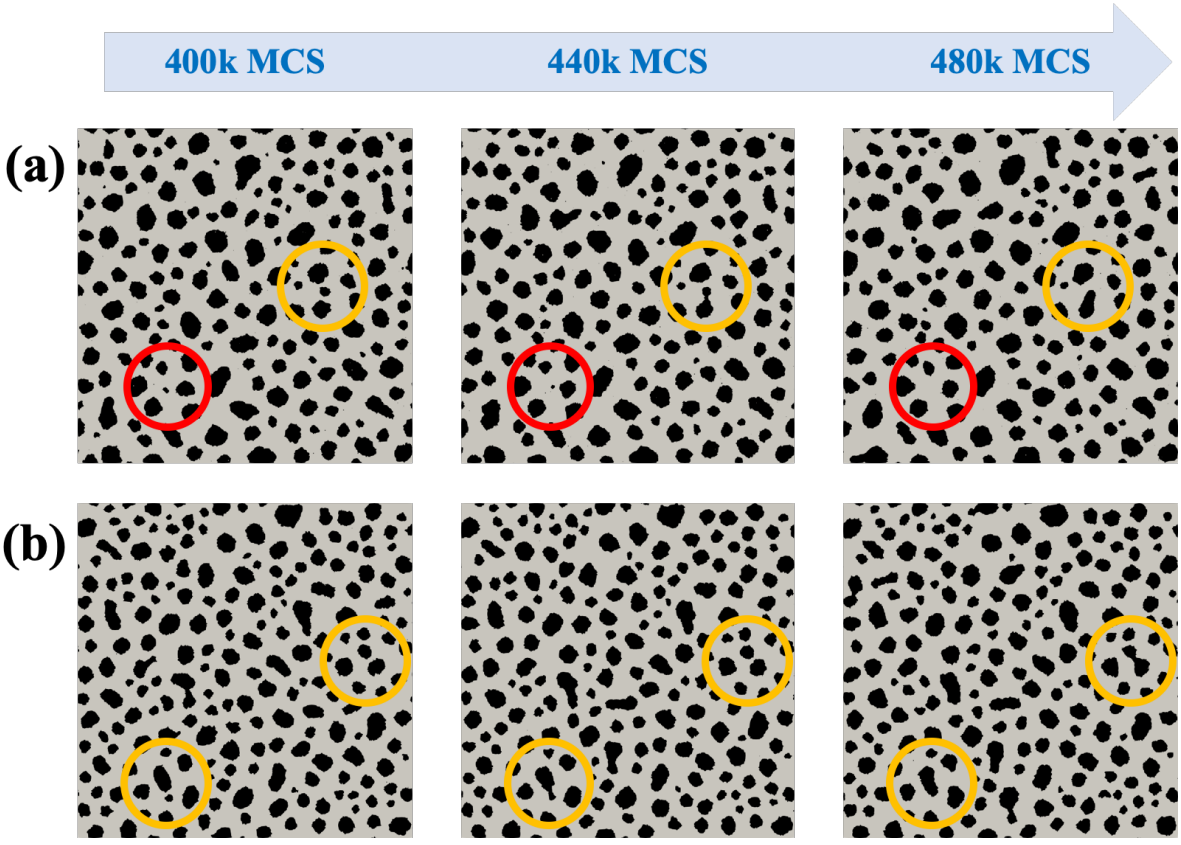

Figure 12. Snapshots of morphological changes as a function of simulation time. Solid pixels and medium pixels are shown in black and gray, respectively. (a) is Kawasaki model (D_{diss} = 1.0) and (b)

is proposed model (D_{diss} = 0.0), and both systems have simulation temperature (kT) with 1.0 and solid area fraction with 0.3.

3.3.2 Kinetic evolution

For a long simulation time, the characteristic length has relationship with simulation time as

$$R^n \sim kt \tag{14}$$

where R is characteristic length, t is simulation time, n is kinetic exponent, and k is rate constant. Here, we modify the equation to a logarithmic function.

$$\ln R = \frac{1}{n}\ln t + \frac{1}{n}\ln k \tag{15}$$

R values are calculated by each of the three methods shown above, and n values, the reciprocal of the slope by linear fitting, are calculated using $\ln R$ and t. At this point, the second linear fitting equation is newly obtained from a section where the difference between the value of the first fitted line and the actual calculated $\ln R$ is less than 1%, reducing the error occurring in front of the simulated data.

3.3.2.1 Change of the characteristic lengths

In Figure 13, we can observe the changes in microstructure over time and the corresponding changes in structure factor $S(\boldsymbol{k}, t)$ and pair correlation function $G(\boldsymbol{r}, t)$. As the ligament size of the microstructure grows, the structure factor image gradually concentrates in the middle, and in the pair correction function image the size of the middle circle gradually increases.

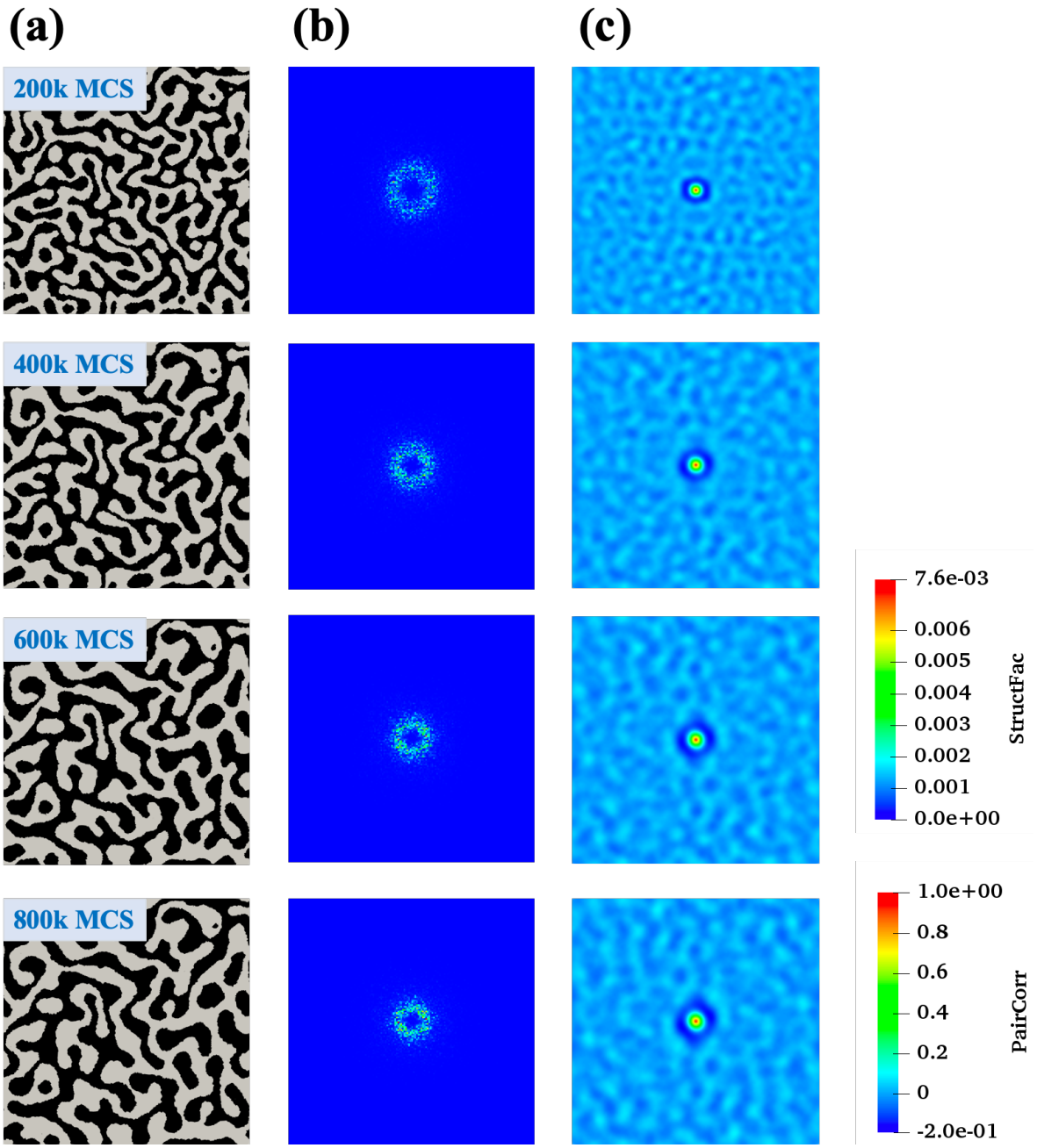

Figure 13. Snapshots of (a) morphological changes (b) structure factor $S(\boldsymbol{k},t)$ and (c) pair correlation function $G(\boldsymbol{r},t)$ of proposed model as a function of simulation time. Solid pixels and medium pixels are shown in black and gray, respectively. Simulation temperature (kT) is 1.0 and solid area fraction is 0.5.

We calculated the characteristic length using the three methods described above and observed its change over time at each temperature. Figure 14 was calculated using the intercept method, Figure 15 using the structure factor and Figure 16 using the pair correlation function. In the structure factor method, the reciprocal of the first moment of $s(k,t)$, a normalized and circularly averaged structure

factor, is used as a characteristic length. As shown in Figure 15 – (a), the graph gradually moves to the left and the height increases. In addition, the r value of $g(r,t)$, a normalized and circularly averaged pair correlation function, that changes from positive to negative is used as the characteristic length in pair correlation function $G(\boldsymbol{r},t)$. In Figure 16 – (a), the graph gradually moves to the right, and the length increases. It is possible to quantitatively identify the changes in length observed by the image in the previous section. In all three methods, the value of characteristic length calculated each method over time increases gradually, and the higher the temperature, the longer the length. The calculated length itself differs from method to method, whereas, the calculated average ratio from each method has a constant value as shown in Figure 17, and also the error values, the standard deviation throughout the entire time of the simulation are very small. As a result, the calculated length is all different, but shows that all methods can be used to calculate a characteristic length. From the next section, the kinetic results are analyzed through the length calculated using the structure factor among the three methods, calculated by the equation with less human-error.

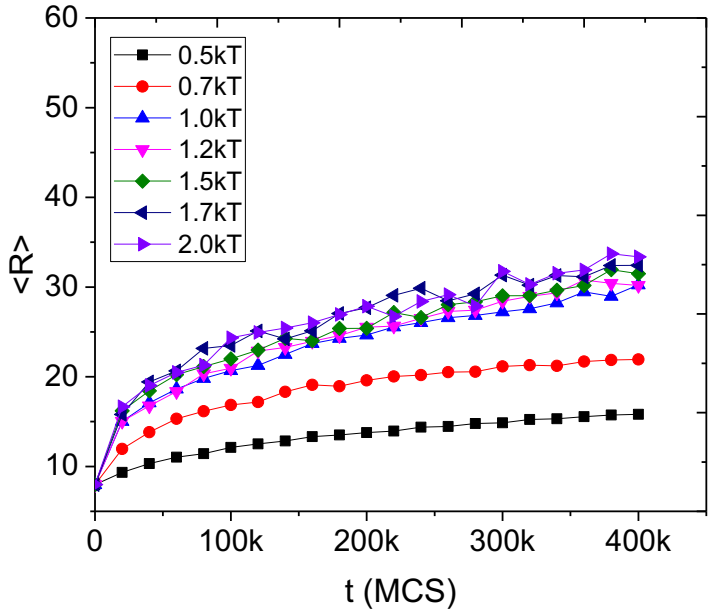

Figure 14. Change of characteristic lengths of proposed model using intercept method over simulation. Simulation temperature (kT) is range from 0.5 to 2.0 and solid area fraction is 0.5.

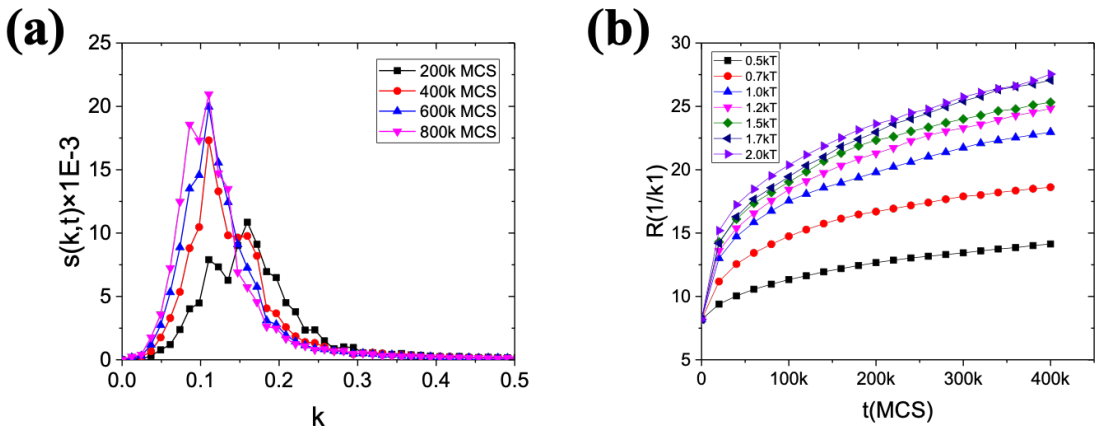

Figure 15. (a) Change of $s(k,t)$ of proposed model with 1.0 simulation temperature and 0.5 solid area fraction over MCS. (b) Change of characteristic lengths of proposed model using structure factor over simulation. Simulation temperature (kT) is range from 0.5 to 2.0 and solid area fraction is 0.5.

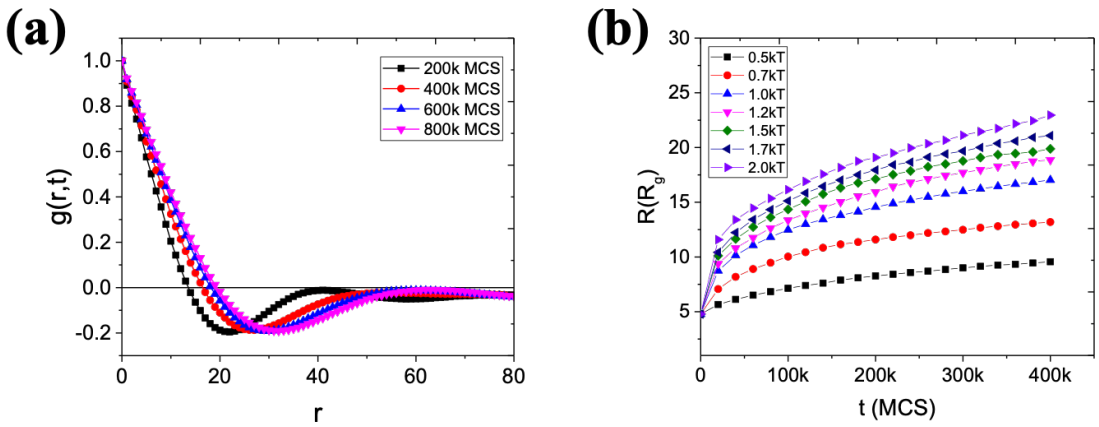

Figure 16. (a) Change of $g(r,t)$ of proposed model with 1.0 simulation temperature and 0.5 solid area fraction over MCS. (b) Change of characteristic lengths of proposed model using pair correlation function over simulation. Simulation temperature (kT) is range from 0.5 to 2.0 and solid area fraction is 0.5.

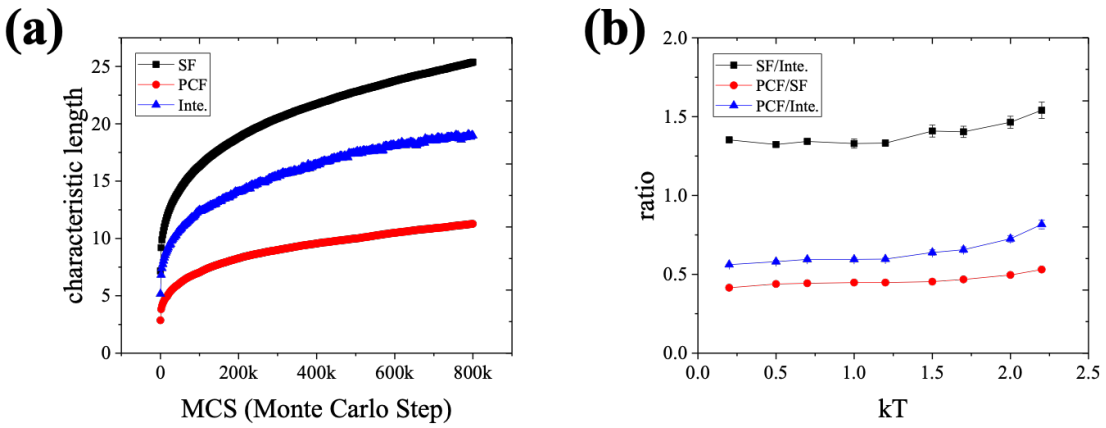

Figure 17. (a) Change of characteristic lengths of proposed model using three methods over MCS. Simulation temperature (kT) is 1.0 and solid area fraction is 0.5. (b) The average ratio of each characteristic length to the total simulation time for each temperature, and the error bar is the standard deviation for the entire simulation time.

3.3.2.2 Effect of temperatures

The value of the kinetic exponent, n, was derived using R obtained from structure factor. In Figure 18, the value of n tends to decrease gradually as the simulated temperature increases. In a low temperature interval, it is difficult to produce a detached pixel due to the small kT value, therefore, bulk diffusion occurs rarely. This is why the n values of the two models are similar, despite of the D_{diss} value of 1 and 0, respectively. However, as the simulation temperature rises, the differences of n between the Kawasaki model, growing with bulk diffusion and surface diffusion, and the proposed model, only growing with surface diffusion, are clearly distinguished. The model using Kawasaki dynamics have an average value of 3 to 5, whereas the proposed model in the range of 4 to 5.

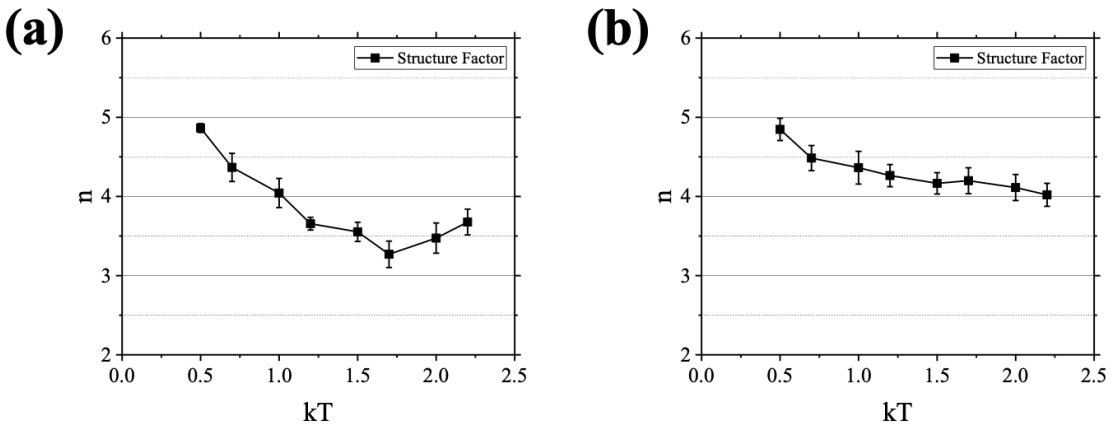

Figure 18. Change of kinetic exponent from structure factor in the variation of temperature and the error bar is the standard deviation for the five repeated simulation. (a) Kawasaki model and (b) proposed model with 0.5 solid area fraction. The error bar is the standard deviation for 5 different simulation domain.

3.3.2.3 Effect of area fraction

The changes in n values resulting from different solid area fractions, both models can be grouped in two large groups, high area fraction as blue and low area fraction as yellow in Figure 19. In the case of small area fraction, the morphologies of the microstructure are not connected to each other but presented in each particle, and connectivity is created from 0.4 and higher area fraction. However, especially on Kawasaki model, the effect of area fraction is reduced as the temperature rises, because the D_{diss} value is 1.0 and it is possible to grow into a bulk diffusion. In microstructure with small area fraction, the probability of meeting between the particles and growing to the larger one decreases; therefore, the Kawasaki model is less affected by area fraction than the proposed model.

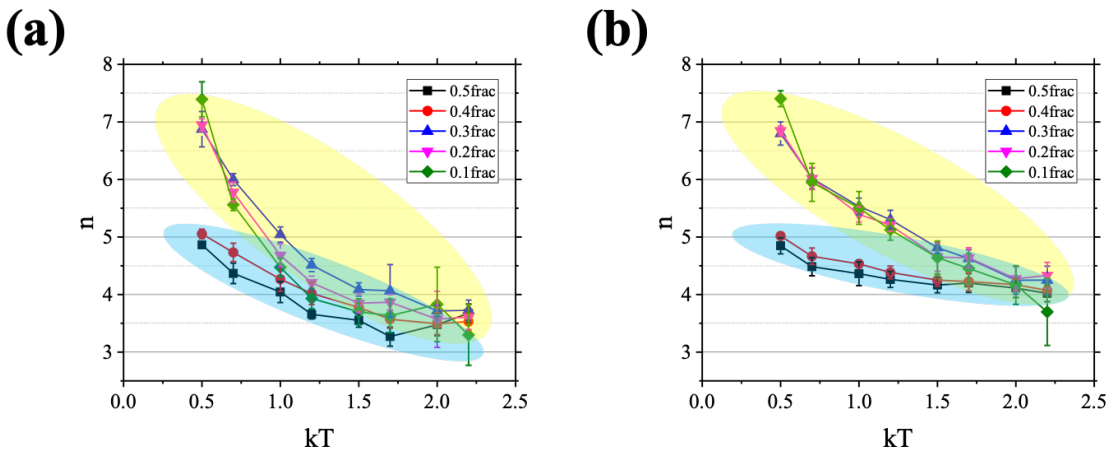

Figure 19. Change of kinetic exponent from structure factor in the variation of temperature, and the error bar is the standard deviation for the five repeated simulation. (a) Kawasaki model and (b) proposed model in 5 different solid area fractions. The error bar is the standard deviation for 5 different simulation domain.

IV. Application to coarsening of bicontinuous porous metal

Many prior studies have shown that nanoporous gold is heat-enhanced by the surface diffusion of gold atom [28-30]. Therefore, we want to compare the kinetics of the model we proposed with the nanopious gold, grown with surface diffusion, and verify the validity of our proposed model. For comparison with actual materials, the two-dimensional model that we have introduced in former chapter, is expanded to three-dimensional model to compare with the nanoporous gold structures.

4.1 Methods

4.1.1 Experimental methods

Np–Au samples were fabricated from Au–Ag precursor alloys (30 at.% Au–70 at.% Ag), which were prepared from high purity Au (99.99%) and Ag (99.99%) pellets by melting at 1100 °C for 30 min, and homogenization was performed at 800 °C for 72 h under pure N_2 environment. Precursor alloys were cut into slices, polished on one side up to 1 μm diamond suspension, and annealed at 800 °C for 24 h to relieve stress. The samples were immersed in 35% nitric acid solution at 80 °C for 72 h for free corrosion dealloying. We obtained coarsened np-Au samples by heat treatment at 450 °C and 600 °C for 0.5h, 1h, 2h, and 6h. Np−Au samples were examined by field emission scanning electron

microscopy (FE-SEM, FEI Nanolab 230) for imaging and measuring ligament size which is diameters of necks, possibly the thinnest parts in connecting ligaments. 2D cross-sectional slice images were obtained for comparing with results from simulation by using focused ion beam (FIB, FEI quanta 3D FEG). Before cross-sectioning, the epoxy was infiltrated into np-Au structure, thereby all pores were filled by epoxy, which makes it possible to blind visible ligaments located under-surface and clearly define boundaries between ligaments and pores.

4.1.2 Simulation methods

In this work, an initial configuration is configured by randomly assigning voxel spins in each phase under various conditions, with a solid area fraction of 0.3 and in the range of 0.2 to 2.0 of the system temperatures. To compare with nanoporous gold, we have simulated with condition when only the value of D_{diss} is zero. $256 \times 256 \times 256$ cube lattices are adopted and total simulation time of each systems is 200k Monte Carlo step (MCS). For direct comparison with experimental data, we analyze three-dimensional microstructure with a cross-sectioned two-dimensional images at a total of 10 heights, and the averages of quantities over the 10 cross-sectioned images are presented below.

4.2 Results and discussions

4.2.1 Results of experiments

From Figure 20 and Figure 21, we can see how much microstructure grows with annealing time and temperature. At 450 °C, the growth rate is very slow over time, but at 600 °C you can see that it is growing fast. To quantitatively calculate the kinetics, we looked at the change in the neck size of ligaments obtained from the experimental data, and the change in size with our intercept method to the SEM image, and derived the n value as shown in Figure 22.

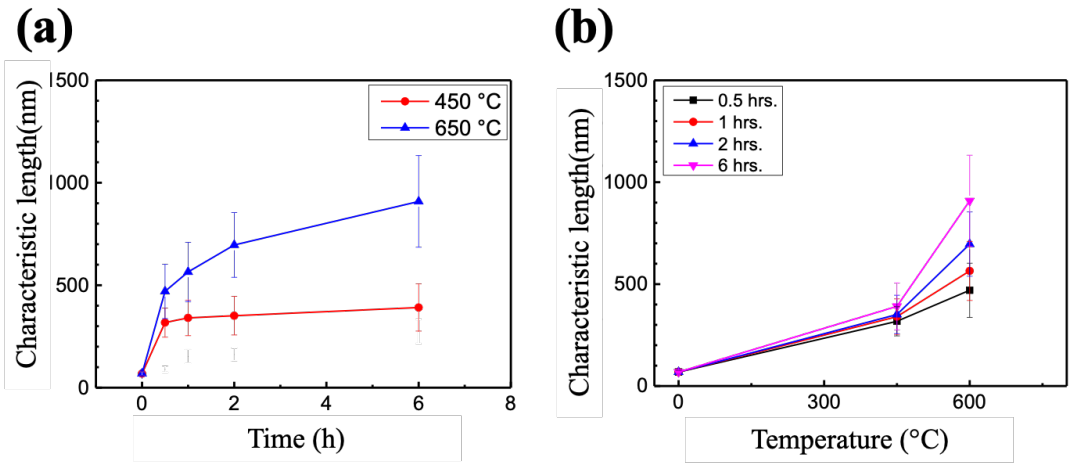

Figure 20. Average ligament size measured by SEM as a function of (a) annealing time and (b) annealing temperature.

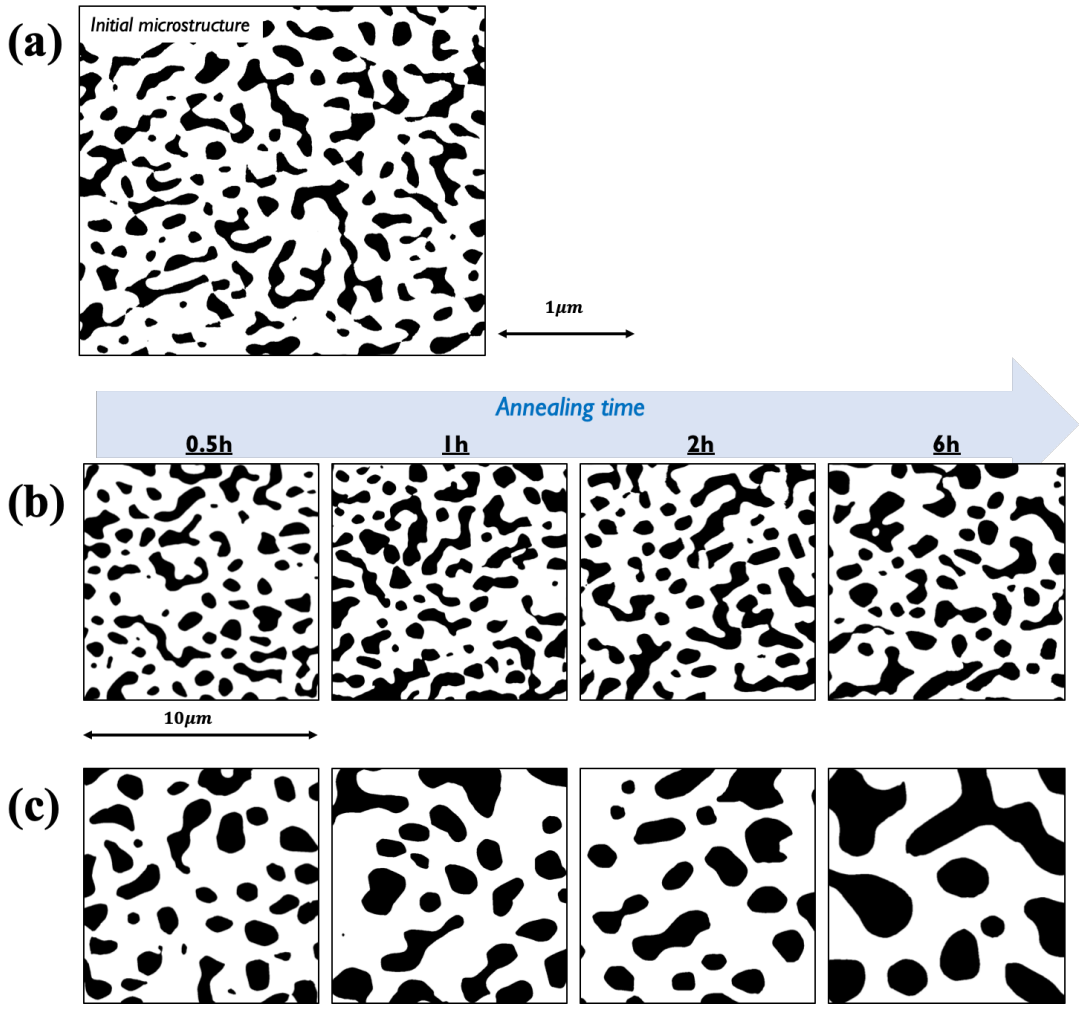

Figure 21. (a) 2D cross-sectional slice SEM image of initial microstructure. Time-dependent change of microstructure (b) at annealing temperature as 450 °C (c) 600 °C.

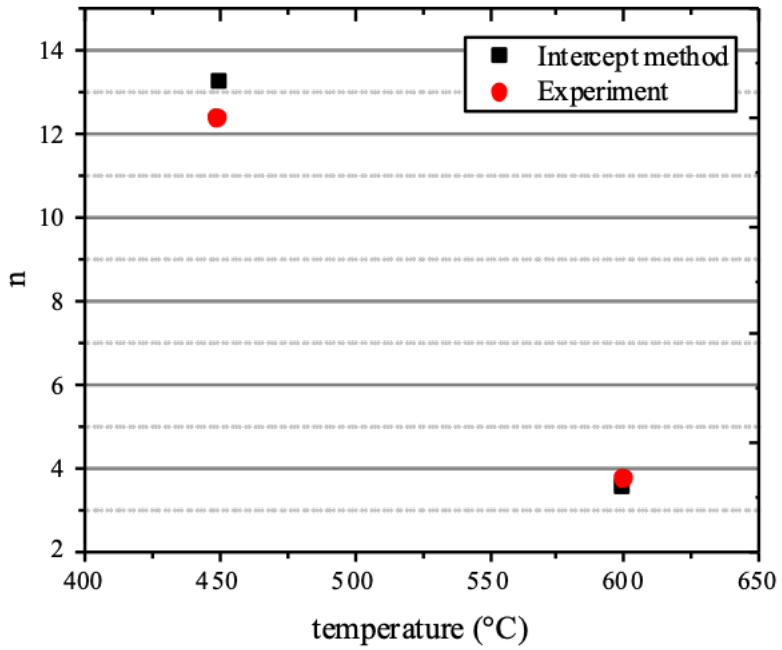

Figure 22. Change of kinetic exponent from intercept method of SEM microstructure and experimental neck size in the variation of temperature.

4.2.2 Results of simulations

Figure 23 and Figure 24 show the morphological evolution of each three-dimensional and two-dimensional cross-sectional microstructure with 0.3 solid area fraction at four different simulation temperature. In the row direction of the figure, we can observe how microstructure grows at each temperature, whereas how much microstructure evolves at each simulation temperature during the same simulation time in the column direction.

To calculate the kinetic exponents, we observed the change in the characteristic length obtained by the intercept method, and using equation 15, calculated the value of n. At this time, the change in value of n according to temperature was fitted into the exponential function to obtain the following relationship,

$$n = 44.13\exp(-3.19kT) + 3.99 \quad (16)$$

where n is kinetic exponent, and kT is simulation temperature.

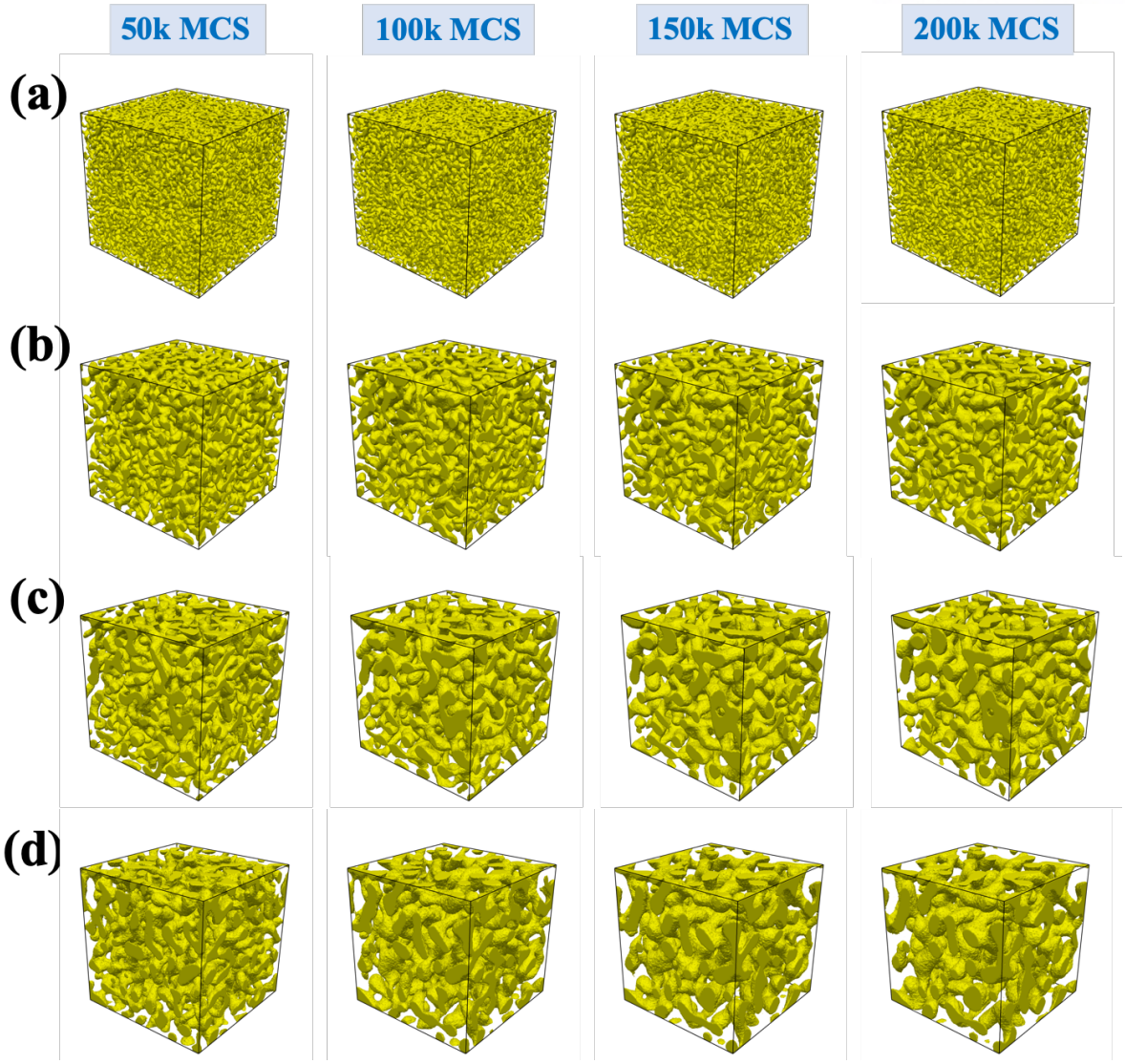

Figure 23. Morphological evolution of 3D microstructure at simulation temperature (kT) is (a) 0.5, (b) 1.0, (c) 1.5, and (d) 2.0

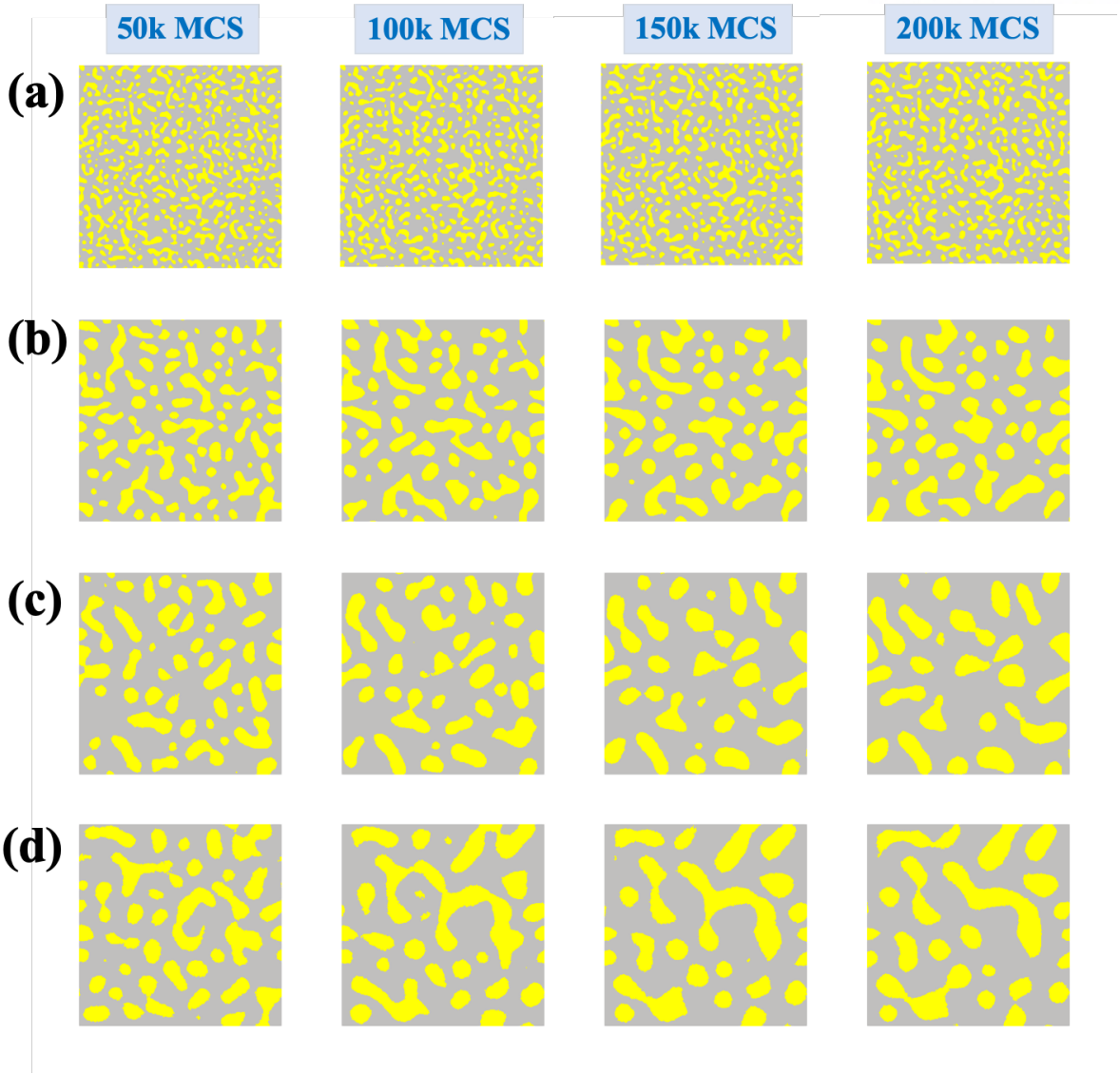

Figure 24. Morphological evolution of 2D cross-sectional slice microstructure at simulation temperature (kT) is (a) 0.5, (b) 1.0, (c) 1.5, and (d) 2.0

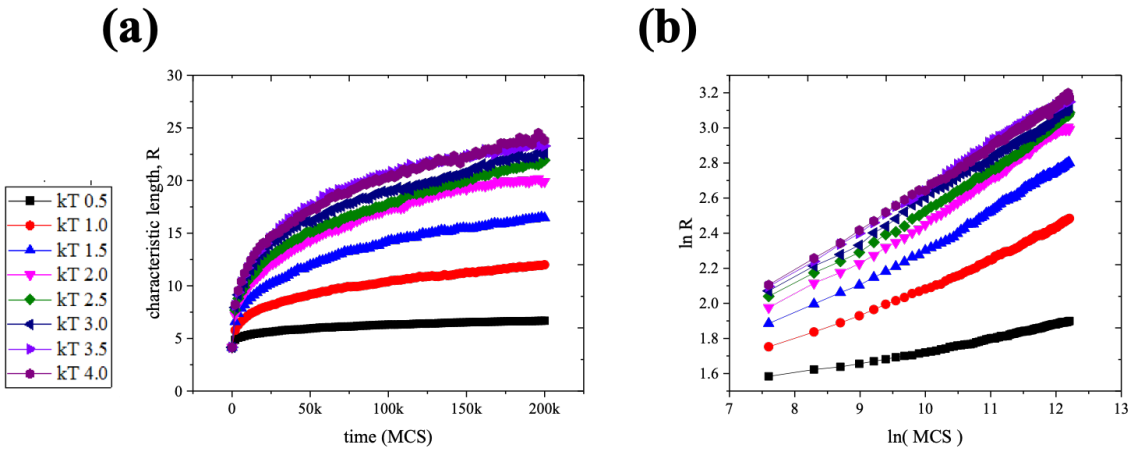

Figure 25. (a) Change of characteristic lengths of proposed model using intercept methods over MCS under various simulation temperature, and (b) is in log scale.

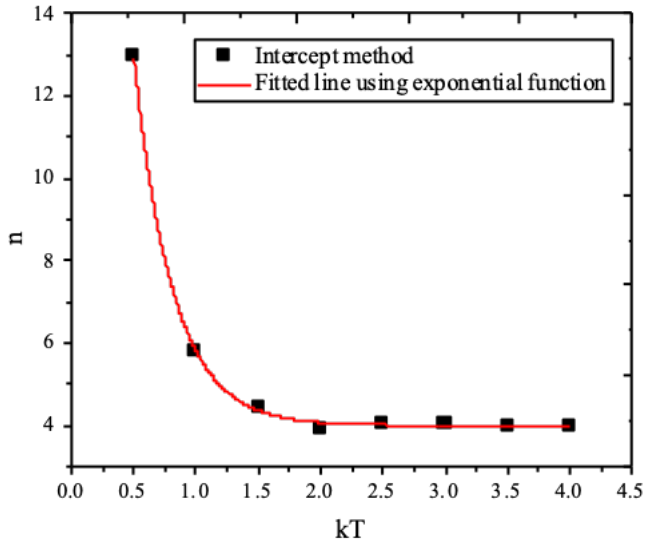

Figure 26. Change of kinetic exponent from intercept method and fitted line using exponential function.

4.2.3 Comparisons of results and discussions

Since Monte Carlo simulations do not have units, direct comparison of experimental results with simulation results is not possible. So, we try to compare the two results using the kinetic exponent and the activation energy. The value of n for the experimental data calculated in the previous section is approximately 12.82, and simulation temperature kT is calculated as approximately 0.52 when put the experimental n, 12.82 into the obtained equation 16.

The activation energy for coarsening Q is described by [28]

$$R \sim exp\ (-\frac{Q}{kT}) \tag{17}$$

where R is the characteristic ligament length; here length from intercept method is used as this characteristic length; k is the Boltzmann's constant, and T is the simulation temperature. At three different simulation time, Q_{sim} is calculated as 0.69 at 100k MCS, 0.72 at 150k MCS, 0.75 at 200k MCS, and average Q_{sim} over time is 0.72 in Figure 27. The Q_{exp} value cited three prior experiment results, and ratio of $exp(-Q_{exp}/RT)$ at 450 °C and 600 °C is 2.60 [29], 2.65 [28] and 3.05 [30], respectively. As a result, in Figure 28, experimental data at 450 °C is equivalent to 0.51 of simulated temperature and 600 °C to range from 1.6 to 2.4. We found that the calculated kinetic exponent value also corresponds to the value calculated through surface diffusion, and that our model is well compliant with existing pre-existing studies.

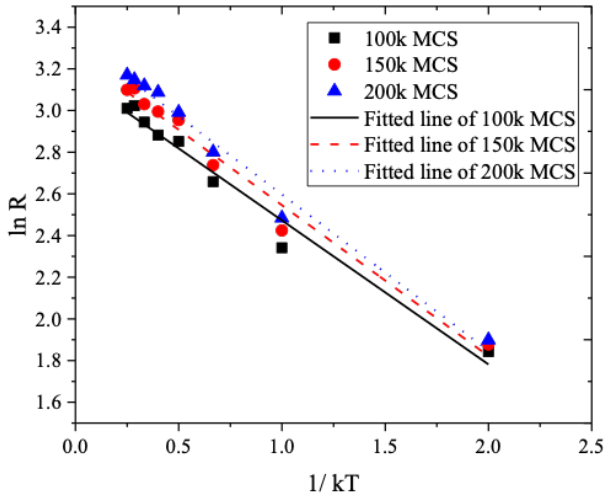

Figure 27. Relation between characteristic length and simulation temperature for calculation of activation energy for thermal coarsening. Average Q_{sim} is calculated as 0.72.

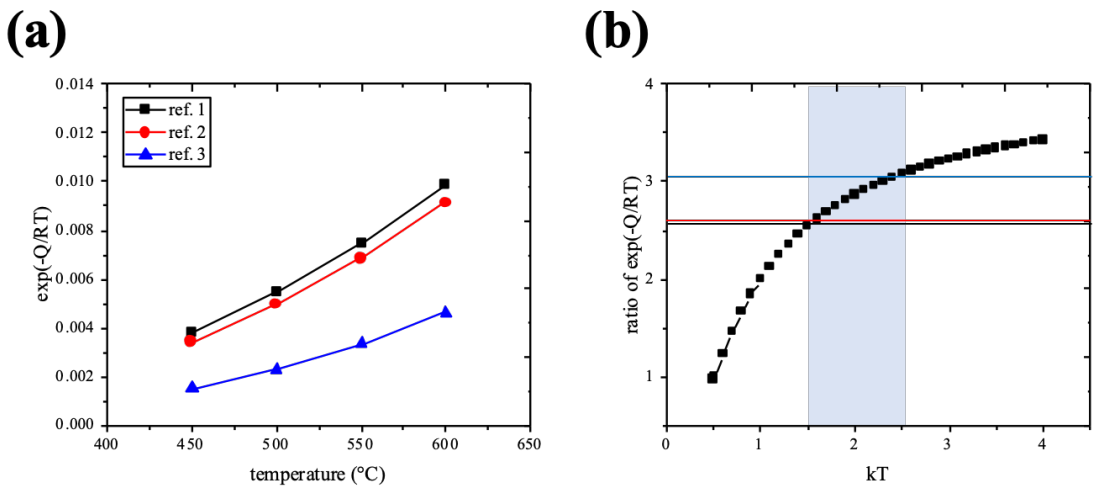

Figure 28. (a) Relationship between $exp(-Q_{exp}/RT)$ and annealing temperature using activation energy Q from ref.1(in black) [29], ref. 2(in red) [28] and ref.3(in blue) [30]. (b) Change of ratio of $exp(-Q_{sim}/kT)$ as a function of kT, and reference lines are in black, red, and blue.

References

1. Lifshitz, I.M. and V.V. Slyozov, *The kinetics of precipitation from supersaturated solid solutions.* Journal of Physics and Chemistry of Solids, 1961. **19**(1): p. 35-50.
2. Wagner, C., *Theorie der Alterung von Niederschlägen durch Umlösen (Ostwald-Reifung).* Zeitschrift für Elektrochemie, Berichte der Bunsengesellschaft für physikalische Chemie, 1961. **65**(7-8): p. 581-591.
3. Bortz, A.B., et al., *Time evolution of a quenched binary alloy: Computer simulation of a two-dimensional model system.* Physical Review B, 1974. **10**(2): p. 535-541.
4. Marro, J., et al., *Time evolution of a quenched binary alloy. II. Computer simulation of a three-dimensional model system.* Physical Review B, 1975. **12**(6): p. 2000-2011.
5. Rao, M., et al., *Time evolution of a quenched binary alloy. III. Computer simulation of a two-dimensional model system.* Physical Review B, 1976. **13**(10): p. 4328-4335.
6. Kostorz, G., *Phase Transformations in Materials*. 2001: Wiley.
7. Sur, A., et al., *Time evolution of a quenched binary alloy. IV. Computer simulation of a three-dimensional model system.* Physical Review B, 1977. **15**(6): p. 3014-3026.
8. Kawasaki, K., *Diffusion Constants near the Critical Point for Time-Dependent Ising Models. I.* Physical Review, 1966. **145**(1): p. 224-230.
9. Yaldram, K. and K. Binder, *Monte Carlo simulation of phase separation and clustering in the ABV model.* Journal of Statistical Physics, 1991. **62**(1): p. 161-175.
10. Yaldram, K. and K. Binder, *Spinodal decomposition of a two-dimensional model alloy with mobile vacancies.* Acta Metallurgica Et Materialia, 1991. **39**(4): p. 707-717.
11. Weinkamer, R., et al., *Using Kinetic Monte Carlo simulations to study phase separation in Alloys.* Phase Transitions, 2004. **77**(5-7): p. 433-456.
12. Fratzl, P. and O. Penrose, *Competing mechanisms for precipitate coarsening in phase separation with vacancy dynamics.* Physical Review B, 1997. **55**(10): p. R6101-R6104.
13. Rogers, T.M., K.R. Elder, and R.C. Desai, *Numerical study of the late stages of spinodal decomposition.* Physical Review B, 1988. **37**(16): p. 9638-9649.
14. Rogers, T.M. and R.C. Desai, *Numerical study of late-stage coarsening for off-critical quenches in the Cahn-Hilliard equation of phase separation.* Physical Review B, 1989. **39**(16): p. 11956-11964.
15. Küpper, T. and N. Masbaum, *Simulation of particle growth and Ostwald ripening via the Cahn-Hilliard equation.* Acta Metallurgica et Materialia, 1994. **42**(6): p. 1847-1858.
16. Chakrabarti, A., R. Toral, and J.D. Gunton, *Late-stage coarsening for off-critical quenches: Scaling functions and the growth law.* Physical Review E, 1993. **47**(5): p. 3025-3038.

17. Furukawa, H., *A dynamic scaling assumption for phase separation.* Advances in Physics, 1985. **34**(6): p. 703-750.
18. Sheng, G., et al., *Coarsening Kinetics of a Two Phase Mixture with Highly Disparate Diffusion Mobility*. Vol. 8. 2010. 249-264.
19. Ling, S. and M.P. Anderson, *Monte Carlo simulation of grain growth and recrystallization in polycrystalline materials.* JOM, 1992. **44**(9): p. 30-36.
20. Aldazabal, J., A. Martín-Meizoso, and J.M. Martínez-Esnaola, *Simulation of liquid phase sintering using the Monte Carlo method.* Materials Science and Engineering: A, 2004. **365**(1-2): p. 151-155.
21. Lee, S., J. Rickman, and A. Rollett, *Three-dimensional simulation of isotropic coarsening in liquid phase sintering I: A model.* Acta Materialia, 2007. **55**(2): p. 615-626.
22. Chen, I.W., G.N. Hassold, and D.J. Srolovitz, *Computer Simulation of Final-Stage Sintering: II, Influence of Initial Pore Size.* Journal of the American Ceramic Society, 1990. **73**(10): p. 2865-2872.
23. Flinn, P.A., *Monte Carlo calculation of phase separation in a two-dimensional Ising system.* Journal of Statistical Physics, 1974. **10**(1): p. 89-97.
24. Ising, E., *Beitrag zur Theorie des Ferromagnetismus.* Zeitschrift für Physik, 1925. **31**(1): p. 253-258.
25. Landau, D.P. and K. Binder, *A Guide to Monte Carlo Simulations in Statistical Physics*. 2009: Cambridge University Press.
26. Metropolis, N., et al., *Equation of State Calculations by Fast Computing Machines.* The Journal of Chemical Physics, 1953. **21**(6): p. 1087-1092.
27. Amar, J.G., F.E. Sullivan, and R.D. Mountain, *Monte Carlo study of growth in the two-dimensional spin-exchange kinetic Ising model.* Physical Review B, 1988. **37**(1): p. 196-208.
28. Jeon, H., et al., *Self-similarity in the structure of coarsened nanoporous gold.* Scripta Materialia, 2017. **137**: p. 46-49.
29. Drechsler, M., J.J. Métois, and J.C. Heyraud, *Surface self-diffusion studied by microscopic measurements of crystallite profile evolutions.* Surface Science, 1981. **108**(3): p. 549-560.
30. Göbel, H. and P. von Blanckenhagen, *A study of surface diffusion on gold with an atomic force microscope.* Surface Science, 1995. **331-333**: p. 885-890.

Acknowledgements

I would like to express gratitude to my advisor Prof. Sukbin Lee for his guidance about my study and research. In addition, I express my appreciation to Prof. Kisuk Lee and Prof. Ju-young Kim for having served on my committee. Their thoughtful questions and comments were valued greatly during the preparation with this thesis. Also, I would like to thank my laboratory members, Youngkyun, Minji, and Myeongjin for helping me in last three years. In addition, I would like to thank all professors at school of materials science and engineering and their lab members.